

Lawrence Berkeley National Laboratory

Recent Work

Title

Cr(VI) Effect on Tc-99 Removal from Hanford Low-Activity Waste Simulant by Ferrous Hydroxide.

Permalink

<https://escholarship.org/uc/item/3wn1h59v>

Journal

Environmental science & technology, 52(20)

ISSN

0013-936X

Authors

Saslow, Sarah A
Um, Wooyong
Pearce, Carolyn I
et al.

Publication Date

2018-10-01

DOI

10.1021/acs.est.8b03314

Peer reviewed

Cr(VI) Effect on Tc-99 Removal from Hanford Low-Activity Waste Simulant by Ferrous Hydroxide

Sarah A. Saslow¹, Wooyong Um^{1,*}, Carolyn I. Pearce¹, Mark E. Bowden², Mark H. Engelhard², Wayne L. Lukens³, Dong-Sang Kim¹, Michael J. Schweiger¹, and Albert A. Kruger⁴

¹*Pacific Northwest National Laboratory, 902 Battelle Blvd, Richland, WA, 99352, USA*

²*Environmental Molecular Sciences Laboratory, Pacific Northwest National Laboratory, Richland, WA, 99354, USA*

³*Lawrence Berkeley National Laboratory, 1 Cyclotron Rd, Berkeley, CA, 94720 USA*

⁴*United States Department of Energy, Office of River Protection, P.O. Box 450, Richland, WA 99352, United States*

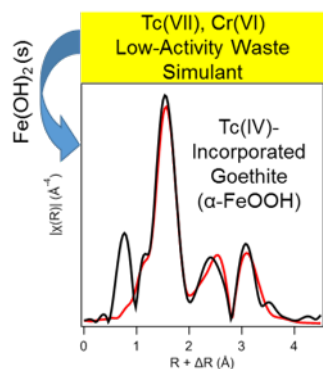
*Corresponding author: Wooyong Um, Pacific Northwest National Laboratory, 902 Battelle Blvd., PO Box 999, P7-54, Richland, WA 99352, USA. Telephone: (509)-371-7175. Fax: (509)-371-7344. Email address: wooyong.um@pnnl.gov. Now at Pohang University of Science and Technology (POSTECH); Email address: wooyongum@postech.ac.kr

Abstract

Here, Cr(VI) effects on Tc-immobilization by Fe(OH)₂(s) are investigated while assessing Fe(OH)₂(s) as a potential treatment method for Hanford low-activity waste destined for vitrification. Batch studies using simulated low-activity waste indicate that Tc(VII) and Cr(VI) removal is contingent on reduction to Tc(IV) and Cr(III). Furthermore, complete removal of both Cr and Tc depends on the amount of Fe(OH)₂(s) present, where complete Cr and Tc removal requires more Fe(OH)₂(s) (~200 g/L of simulant), than removing Cr alone (~50 g/L of simulant).

XRD analysis suggests that $\text{Fe}(\text{OH})_2(\text{s})$ reaction and transformation in the simulant produces mostly goethite ($\alpha\text{-FeOOH}$), where $\text{Fe}(\text{OH})_2(\text{s})$ transformation to goethite rather than magnetite is likely due to the simulant chemistry, which includes high levels of nitrite and other constituents. Once reduced, a fraction of Cr(III) and Tc(IV) substitute for octahedral Fe(III) within the goethite crystal lattice as supported by XPS, XANES, and/or EXAFS results. The remaining Cr(III) forms oxide and/or hydroxide phases, whereas Tc(IV) not fully incorporated into goethite persists as either adsorbed or partially incorporated Tc(IV)-oxide species. As such, to fully incorporate Tc(IV) into the goethite crystal structure, additional $\text{Fe}(\text{OH})_2(\text{s})$ (>200 g/L of simulant) may be required.

TOC



1. Introduction

Technetium-99 (Tc) is a radioactive fission product present at nuclear waste legacy sites that is problematic due to its long half-life (2.1×10^5 years), high fission yield ($\sim 6\%$), and environmental mobility as Tc(VII) species in oxidizing environments.¹⁻³ Unfortunately, nuclear waste treatment and environmental remediation strategies targeting Tc are hindered by current high temperature treatment technologies and the presence of co-mingled redox-active competitors, e.g. Cr(VI).⁴⁻⁵ For example, at the US Department of Energy Hanford Site (Washington State, USA) the baseline treatment plan for nuclear waste is vitrification,⁶⁻⁷ which requires operating temperatures >1000 °C that consequently causes Tc volatilization and low Tc-retention in the glass waste form. One strategy to overcome Tc volatilization is reduction of Tc(VII) to stable Tc(IV) with concurrent Tc(IV) incorporation into minerals,⁷⁻¹⁴ although this treatment method is often complicated by the presence of co-mingled Cr(VI), which was used as a corrosion inhibitor in Hanford nuclear waste storage tanks.⁴ Cr(VI) has a more favorable reduction potential, -0.16 V vs -0.36 V for Tc(VII) at pH 14,¹⁵⁻¹⁶ and exists in Hanford nuclear waste streams at concentrations orders of magnitude greater than Tc.¹⁷ As a result, reductants added to reduce Tc(VII) are consumed by Cr(VI). Thus, there remains a critical need for treatment technologies that can reduce Tc(VII) in the presence of Cr(VI).

In a preliminary study, ferrous hydroxide solid ($\text{Fe}(\text{OH})_2(\text{s})$) was successfully used to reduce Tc(VII) in the presence of Cr(VI) and incorporate Tc(IV) into magnetite via $\text{Fe}(\text{OH})_2(\text{s})$ mineral transformation under oxic conditions.¹⁸ This work was performed under the high ionic strength and pH conditions expected for Hanford low-activity waste (LAW) streams, but used a simple solution chemistry that only considered Tc(VII) and Cr(VI) in 1 M NaOH. Here, $\text{Fe}(\text{OH})_2(\text{s})$ is used to treat Tc in a simulated LAW solution, to assess (i) how complex and realistic waste

streams affect the efficacy of this approach and (ii) provide mechanistic evidence for Cr(VI) reduction and solid formation and how this impacts the $\text{Fe}(\text{OH})_2(\text{s})$ treatment mechanism for Tc. Hanford's liquid radioactive/chemical waste, currently stored in tanks but destined for pretreatment and vitrification, varies from tank to tank due to the different separation processes used for spent nuclear fuel, resulting in complex mixtures of nitrate, nitrite, phosphate, sulfate, and organic based solvents.¹⁹ As such, the exact LAW composition for treatment is not known, so for the purpose of this work, an overall average LAW simulant composition is used based on output from the Hanford Tank Waste Operations Simulator (HTWOS) model.¹⁷ To arrive at this average composition, which includes nitrate, nitrite, sulfate, aluminum, Cr(VI) and other minor constituents, the HTWOS model tracks tank waste storage, retrieval, and multiple treatment and immobilization processes over ~20 years of operation.

The treatment approach described here involves reduction of Tc(VII) in the presence of Cr(VI) and removal of Tc from solution through incorporation into a solid iron oxide/hydroxide phase. Once reduced and stabilized, Tc is expected to be resistant to release from the iron oxide/hydroxide product(s), which may stabilize Tc during vitrification and increase Tc loading into glass. In addition, development and implementation of this approach could improve environmental remediation efforts that target co-mingled Tc(VII) and Cr(VI) contaminated areas.²¹

2. Experimental

$\text{Fe}(\text{OH})_2(\text{s})$ Synthesis. A detailed synthesis procedure for $\text{Fe}(\text{OH})_2(\text{s})$ and product characterization may be found in previously published work.¹⁸ Briefly, $\text{Fe}(\text{OH})_2(\text{s})$ was prepared and stored inside an anoxic chamber (Coy Laboratories) that was maintained using a gas mix of N_2 (98%) and H_2 (2%). $\text{Fe}(\text{II})\text{Cl}_2 \cdot 4\text{H}_2\text{O}$ (14 g, >95%, Fisher Scientific) was dissolved in N_2 -

purged double deionized water (400 g, DDI, Millipore 18 Ω). Dissolved Fe(II) was then precipitated as Fe(OH)₂(s) by adding 8.2 mL of 10 M NaOH (Fisher Scientific) to solution and mixing by hand. The solid was allowed to react overnight and then separated from the supernatant using a 0.45 μ m Nalgene® filter. The Fe(OH)₂(s) was then allowed to dry for 24 hours before it was powdered using a mortar and pestle.

Simulant Preparation. A 5 M Na Hanford LAW simulant with 1080 ppm Cr(VI) was generated as described previously,¹⁷ and spiked with 1-100 ppm Tc(VII), using a 10,000 mg/L Tc stock solution (NH₄TcO₄). The starting simulant was characterized using ion chromatography (IC) and inductively coupled plasma optical emission spectrometry (ICP-OES) (Table 1).

Table 1. 5 M Na Average LAW Simulant Composition

Constituent	Target Concentration [mg/L]*	Measured Concentration [mg/L]	Constituent	Target Concentration [mg/L]*	Measured Concentration [mg/L]
Al	8280	8500	F ⁻	600	<1000
Cr	1120	1080	Cl ⁻	1500	<2500
P	1520	981	NO ₂ ⁻	26,000	26,800
K	1280	1300	Br ⁻	-	<5000
Na	115,000	110,000	NO ₃ ⁻	101,000	102,000
S	2740	2810	SO ₄ ⁻	-	10,100
Ti	-	7.84	PO ₄ ⁻	-	<7500
pH		13.5	E _h (SHE)		26 – 81 mV

* Target Concentrations from Russell et al, 2013 for 5 M Na Average LAW Simulant;¹⁷ target and measured concentrations determined using IC and ICP-OES.

-: Not identified

(SHE): Standard Hydrogen Electrode corrected

Tc(VII) and Cr(VI) Treatment by Fe(OH)₂(s). Fe(OH)₂(s) (~0.1-1.2 g) was added to LAW simulant to achieve final Fe(OH)₂(s):simulant ratios between 1 and 360 g/L. Fe(OH)₂(s) was removed from the anaerobic chamber immediately before simulant addition, after which sample(s) reacted for 3 days (\pm 1 hour) in an oven set to 75 °C with occasional hand mixing. In some instances, aliquots of Fe(OH)₂(s) were added sequentially over the reaction period.¹⁸ For these samples, each aliquot of Fe(OH)₂(s) was allowed to react with the simulant for ~24 hours

before sampling and subsequent $\text{Fe}(\text{OH})_2(\text{s})$ addition. After 3 days, all samples were allowed to cool for ≥ 2 hours before the solid product was separated from the supernatant (0.45 μm Nalgene® filter), rinsed with ~ 50 mL of DDI, and air-dried for ≥ 24 hours. The supernatant was analyzed to determine final Cr (ICP-OES) and Tc (ICP-MS) concentrations. The final pH of a representative set of supernatants was 13.5 ± 0.1 and the E_h (SHE) ranged from 26 to 81 mV before and after the 3 day reaction period.

X-ray Photoelectron Spectroscopy (XPS). Samples were prepared by dusting carbon tape with dry sample powder. Tc-free samples were analyzed using a Physical Electronics Quantera Scanning X-ray Microprobe equipped with a focused monochromatic Al $K\alpha$ X-ray (1486.7 eV) source for excitation and a spherical section analyzer. Tc-containing samples were analyzed using a Kratos Axis DLD spectrometer with a monochromatic Al $K\alpha$ X-ray source. An 80 W X-ray beam was focused to 100 μm (diameter) and scanned over the sample. High-energy resolution spectra were collected using a pass-energy of 69.0 eV and 0.125 eV step size. Spectra were charge-corrected to the main line, carbon 1s peak at 285.0 eV. Data analysis and peak fitting was performed in CasaXPS (version 2.3.15) (see SI for details).

X-ray Diffraction (XRD). XRD patterns were collected using a Rigaku Miniflex II XRD unit equipped with a Cu $K\alpha$ radiation ($\lambda=1.5418$ Å, 30-40 kV, 15 mA) source. Samples were scanned, at minimum, between 3 – 90 degrees 2θ at 0.5 degrees/min using a 0.02 degree step size. Reitveld quantification refinements were performed for each pattern collected (see SI for details).

X-ray Absorption Near Edge Structure (XANES) and Extended X-ray Absorption Fine Structure (EXAFS) Spectroscopy. Tc K-edge (21,044 eV) spectra were collected on beamline 11-2 at the Stanford Synchrotron Radiation Laboratory (SSRL) for samples spiked with Tc

concentrations ≥ 100 mg/L. Cr K-edge (5,989 eV) spectra were collected on SSRL beamlines 11-2 and 4-1. Dead-time correction and data reduction was performed using SixPack.²² Data analysis was performed using ATHENA/ARTEMIS software.²³ Tc XANES spectra were energy calibrated using a Tc(VII) reference (pertechnetate (TcO_4^-) adsorbed on Reillex-HPQ polymer resin) and fit using a linear combination of Tc(IV) and Tc(VII) standards.^{14, 24-25} For EXAFS fitting, a Tc-substituted goethite ($\alpha\text{-FeOOH}$) structure was used in addition to models for $\text{TcO}_2 \cdot 2\text{H}_2\text{O}$ and TcO_4^- as necessary. Cr XANES spectra were energy calibrated using a Cr foil reference and fit using a linear combination of Cr(III) and Cr(VI) standards. Additional sample preparation and analysis details are provided in the SI.

3. Results and Discussion

Tc(VII) and Cr(VI) Removal by $\text{Fe}(\text{OH})_2(\text{s})$. A viable material for removing contaminants from LAW must stabilize Tc with as little solid as possible to meet glass composition constraints and avoid costly operational changes. The minimum $\text{Fe}(\text{OH})_2(\text{s})$ required to remove co-mingled Tc and Cr from the LAW simulant was determined as a function of $\text{Fe}(\text{OH})_2(\text{s})$:simulant ratio (Figure 1). Studies performed without Tc indicate that 50 g of $\text{Fe}(\text{OH})_2(\text{s})$ per liter of simulant is required to remove Cr (1080 ppm) from solution. The addition of 1 ppm Tc does not change the minimum $\text{Fe}(\text{OH})_2(\text{s})$ required to remove Cr(VI); though to remove $>97.6\%$ Tc requires at least 200 g $\text{Fe}(\text{OH})_2(\text{s})$ per liter of simulant.

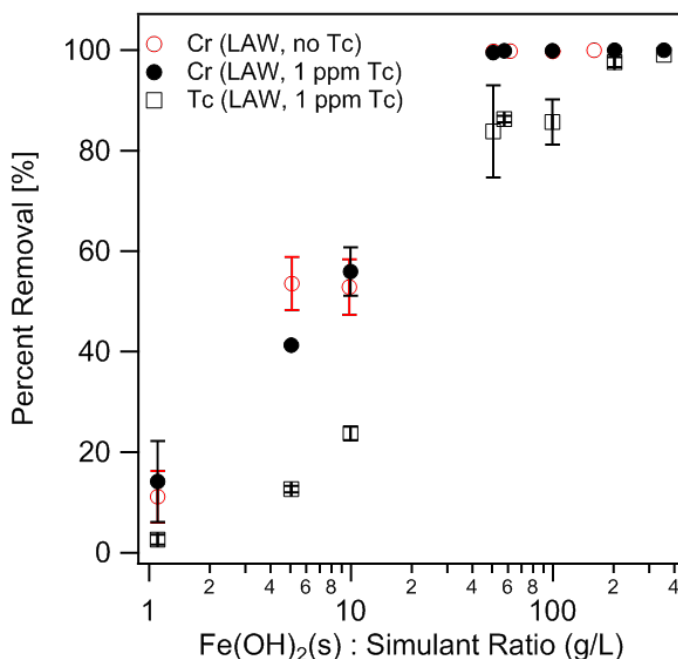


Figure 1. Cr and Tc removal from LAW simulant with 1 ppm Tc (black) and without Tc (red). Cr(VI) results are indicated by filled or open circles, Tc results by open squares. Error bars represent the standard deviation of results averaged from two to six replicate samples. Percent removal assumed to be 100% if below ICP-OES detection limit for Cr (23 μ g/L) or ICP-MS detection limit for Tc (33 ng/L).

To better understand the additional $\text{Fe}(\text{OH})_2(\text{s})$ requirement needed to remove Tc(VII) from the LAW simulant, the solution chemistry and redox and transformation processes must be considered. Similar to the 1 M NaOH system,¹⁸ the experimentally determined amount of $\text{Fe}(\text{OH})_2(\text{s})$ needed to remove Tc (1 ppm) and Cr (1080 ppm) is $\sim 35\times$ more than the amount needed to reduce Tc(VII) to Tc(IV), and Cr(VI) to Cr(III), based solely on redox requirements. This is partially attributed to rapid oxidation of Fe(II) to Fe(III) by air and the additional Fe(II) needed to form iron oxide/hydroxide phases that incorporate Tc and/or Cr,^{10, 26-29} but is likely also the result of the complex chemical environment, e.g., pH and competing contaminants in the LAW simulant that require excess reductant due to competing chemical processes. For instance, the Tc and Cr Pourbaix diagrams (see SI) for the simulant solution (Table 1), assuming 200 g of $\text{Fe}(\text{OH})_2(\text{s})$ per liter, suggest that both constituents should remain in solution as oxidized TcO_4^-

and CrO_4^{2-} given the pH and E_h conditions measured before $\text{Fe}(\text{OH})_2(\text{s})$ addition and after the 3 day reaction period. The Pourbaix diagrams predict that $\text{Fe}(\text{II})$ would preferentially facilitate the reduction and volatilization of nitrate and nitrite as $\text{N}_2(\text{g})$, with the remaining $\text{Fe}(\text{II})$ precipitating as the spinel hercynite $(\text{Fe}(\text{II})\text{Al}(\text{III})_2\text{O}_4)$.³⁰⁻³¹ Yet, at a 200 g/L $\text{Fe}(\text{OH})_2(\text{s})$:simulant ratio, neither Tc nor Cr are detected in solution at significant concentrations. Additionally, IC measurements of the remaining solution indicate negligible removal of nitrate and only ~45% removal of nitrite. $\text{Al}(\text{III})$ removal was determined to increase by ~45% with increasing $\text{Fe}(\text{OH})_2(\text{s})$:simulant ratio as determined by ICP-OES analysis, but was not completely removed as thermodynamics would predict in the Pourbaix diagrams. In the absence of *in situ* E_h measurements during reaction, these measurements demonstrate that the reduction potential of the simulant solution was significantly lowered upon addition of $\text{Fe}(\text{OH})_2(\text{s})$. Furthermore, kinetic processes may overcome thermodynamics early in the reaction, and as a result of these competing processes Tc and Cr are removed from solution.

Additional evidence for both a thermodynamically- and kinetically-driven system is that Tc removal is not contingent on complete $\text{Cr}(\text{VI})$ removal from the LAW simulant. Both contaminants are removed concurrently, despite a more favorable reduction potential for $\text{Cr}(\text{VI})$ versus $\text{Tc}(\text{VII})$.³² This behavior is evident in [Figure 1](#), where, between $\text{Fe}(\text{OH})_2(\text{s})$:simulant ratios 5-50 g/L, Tc removal begins before Cr removal has reached ~100%. However, between 50-100 g/L, Tc removal plateaus until the $\text{Fe}(\text{OH})_2(\text{s})$:simulant ratio reaches 200 g/L. This was not seen in the simplified system and could be attributed to the presence of nitrite, which may compete more aggressively for reducing electrons without $\text{Cr}(\text{VI})$ present.

Finally, based on conclusions derived previously, the removal of $\text{Cr}(\text{VI})$ by $\text{Fe}(\text{OH})_2(\text{s})$ in the LAW simulant should be contingent on $\text{Cr}(\text{VI})$ reduction to $\text{Cr}(\text{III})$.¹⁸ Using the IC/ICP-MS

method previously reported³⁰ and detailed in the SI, the speciation of Cr in the final supernatant was determined using stable mass isotope ⁵²Cr. Duplicate experiments with a Fe(OH)₂(s):simulant ratio of 9.8 g/L, a ratio below the requirement for complete Cr(VI) removal, removed only 53(6) % of Cr from the LAW simulant with the rest remaining as Cr(VI) in solution. This alludes to a reduction requirement for Cr(VI) removal that is confirmed via solid characterization in the following sections. Removal of Tc(VII) from solution is also expected to occur via reduction to Tc(IV).

Tc and Cr Immobilization in the Solid Phase

Solid Characterization by XRD: Solid phase(s) identification is critical for drawing mechanistic conclusions from Cr and Tc immobilization. Two Tc-free samples prepared at 50 and 100 g/L Fe(OH)₂:simulant ratios were analyzed by XRD to identify and quantify the minerals formed (Table 2, XRD patterns in the SI). For both samples, goethite (α -FeOOH) accounts for 77% – 81% of the solid despite doubling the Fe(OH)₂(s):simulant ratio. The remaining solid is comprised of feroxyhyte (δ -FeOOH), 14 – 17%, and trace amounts (1 – 6%) of amorphous material and/or hematite (Fe₂O₃). High resolution Fe XPS scans collected from three samples with Fe(OH)₂(s):simulant ratios ranging from 50-200 g/L corroborate these XRD results, where 83-89 atomic % of Fe is present as goethite (Table 2).

Table 2. XRD and High Resolution XPS Analysis of Select Solid Phases

Sample		LAW-50-0Tc-1	LAW-100-0Tc	LAW-200-100Tc
Fe(OH) ₂ (s):Simulant Ratio	g/L	50	100	200
Starting [Tc(VII)]	ppm	0	0	100
XRD Analysis				
Goethite (α -FeOOH)	wt%	77	81	-
a	(\AA) [*]	4.602(2)	4.597(3)	-
b	(\AA) [*]	9.920(3)	9.913(2)	-
c	(\AA) [*]	3.0096(9)	3.0080(9)	-
Crystal Size	(nm) ^{**}	9.8(1)	10.7(1)	-
Feroxyhyte (δ -FeOOH)	wt%	17	14	-
Hematite (Fe ₂ O ₃)	wt%	-	3	-
Amorphous/Unidentified	wt%	6	1	-

<i>Survey XPS Analysis</i> ^{**}				
Cr 2p	<i>at %</i> [*]	1.6(1)	1.1(1)	0.13(1)
Tc 3d	<i>at %</i>	-	-	0.14(3)
Fe 2p	<i>at %</i>	7.3(4)	8.4(8)	1.7(2)
C 1s	<i>at %</i>	27(4)	19(6)	24(1)
O 1s	<i>at %</i>	64(3)	71(5)	74(1)
<i>Cr XPS Analysis</i> ^{**}				
CrOOH	<i>at %</i>	46(1)	38(14)	59(2)
Cr ₂ O ₃	<i>at %</i>	28(10)	43(19)	32(4)
Cr(OH) ₃	<i>at %</i>	24.7(2)	18(5)	1(2)
Cr(VI)	<i>at %</i>	1.5	1.3(5)	8.3(8)
<i>Tc XPS Analysis</i> ^{**}				
Tc(VII)	<i>at %</i>	-	-	52(1)
Tc(IV)	<i>at %</i>	-	-	48(1)
<i>Fe XPS Analysis</i> ^{**}				
FeCr ₂ O ₄	<i>at %</i>	0	0	5.7(2)
Fe ₃ O ₄	<i>at %</i>	12(1)	11(2)	11(1)
FeOOH	<i>at %</i>	88(1)	89(2)	83(1)

(-) No Detected or Analyzed (*) Atomic percent

Goethite (α -FeOOH)³³: a = 4.634 Å, b = 9.945 Å, c = 3.0321 Å

*Values in parentheses are $\pm 3\sigma$, based on the error associated with the Reitveld refinement.

**Values in parentheses are $\pm 1\sigma$. For XPS, the standard deviation is determined from the average of two replicate spot analyses collected for each sample.

The formation of goethite instead of magnetite,^{18, 34-35} or hercynite (as predicted by Pourbaix diagrams presented in the SI), suggests that the solid product is also heavily influenced by co-mingled constituents. As previously mentioned, an Fe(OH)₂(s):simulant ratio of ~200 g/L removes ~45% (~12,200 mg/L) of the simulant nitrite and ~45% of Al(III) (SI Figure S1). As nitrite reduction continues, the ratio of Fe(III) to Fe(II) increases, as does the OH/Fe ratio, both of which favor the formation of goethite over magnetite.³⁶ As goethite forms and Tc(VII) is reduced to Tc(IV), incorporation of Tc(IV) into the goethite structure likely occurs via substitution for Fe(III) due to their identical, six coordinate crystal radii (0.785 Å).^{27, 37-38} Substitution of Tc(IV) is not expected to significantly influence the bulk mineral phase distribution determined by XRD nor change the goethite lattice parameters. Although charge balance via Fe(II) substitution for Fe(III) may expand the lattice at concentrations higher than those tested here.¹⁰

In contrast, Cr(III) and/or Al(III) substitution into goethite would cause a decrease in calculated goethite lattice parameters since the crystal radius of six coordinate Cr(III), 0.755 Å, and Al(III), 0.670 Å, are smaller than Fe(III).^{33, 38-42} Reitveld analysis of collected XRD patterns (Table 2 **Error! Reference source not found.**) provides the unit cell parameters *a*, *b*, and *c* for goethite in the absence of Tc. All parameters decrease relative to unsubstituted goethite with increasing Fe(OH)₂(s):simulant ratio.³³ This trend is indicative of increased substitution for Fe(III) by Cr(III) and/or Al(III) in goethite as both constituents are removed from the simulant (Figure 1 and SI Figure S1).

Bulk Solid Phase Cr Speciation Determined by XANES: Three samples were analyzed by XANES at SSRL to determine the bulk oxidation state and speciation of Cr following reduction and removal by Fe(OH)₂(s) (Figure 2, left panel). As a control, one of the analyzed samples (LAW-50-0Tc) was prepared without Tc and at the minimum Fe(OH)₂(s):simulant ratio needed to remove Cr(VI) from solution, 50 g/L. The remaining two samples were prepared with 100 ppm Tc(VII) at two different Fe(OH)₂(s):simulant ratios: 50 g/L (LAW-50-100Tc) and 200 g/L (LAW-200-100Tc). Linear combination analysis (LCA) of each sample initially considered six possible Cr standards: Cr foil, Cr₂O₃, Cr alum (KCr(SO₄)₂•12H₂O, Cr(III) octahedrally coordinated by water), Fe_{2.5}Cr_{0.5}O₄, FeCr₂O₄, and K₂CrO₄ (Figure 2, middle panel). It is important to note that Cr(III) forms octahedrally coordinated species both in ordered (iron-containing oxides) and disordered environments. According to XRD results (Table 2), Cr would be incorporated into goethite, not spinel phases such as chromite (FeCr₂O₄) or Fe_{2.5}Cr_{0.5}O₄. However, without a Cr-substituted goethite standard, Fe_{2.5}Cr_{0.5}O₄ and FeCr₂O₄ standards are used here to represent the ordered octahedral environment expected for Cr-substituted goethite.⁴³ Furthermore, the disordered octahedral symmetry of Cr(III) in Cr alum⁴⁴ is assumed to represent

255 Cr(III) that has formed separate from the iron phase, e.g., Cr(OH)_3 or an amorphous phase with a
256 similar local structure.⁴⁵ Standards that did not contribute significantly to the LCA fit (value <
257 2σ) were removed and the data refit using the remaining standards. The final Cr LCA results are
258 shown in Table 3.

259 For all samples, the absence of the prominent Cr(VI) pre-edge feature confirms that Cr is
260 present as Cr(III) and supports the proposed solution removal mechanism that requires Cr(VI)
261 reduction to Cr(III). Furthermore, all samples contained Cr alum (35 – 38 %) and $\text{Fe}_{2.5}\text{Cr}_{0.5}\text{O}_4$
262 (58 – 62 %) as the major phases present regardless of Fe(OH)_2 :simulant ratio, although for the
263 two samples with a Fe(OH)_2 (s):simulant ratio of 50 g/L a small contribution of FeCr_2O_4 (6 %) was
264 also determined. Overall, given the low solubility of Cr(III)-containing solids, Cr present in
265 these samples is less susceptible to re-oxidation and release into the environment and exhibits a
266 similar removal mechanism despite changes in Fe(II) resources and Tc(VII) presence.

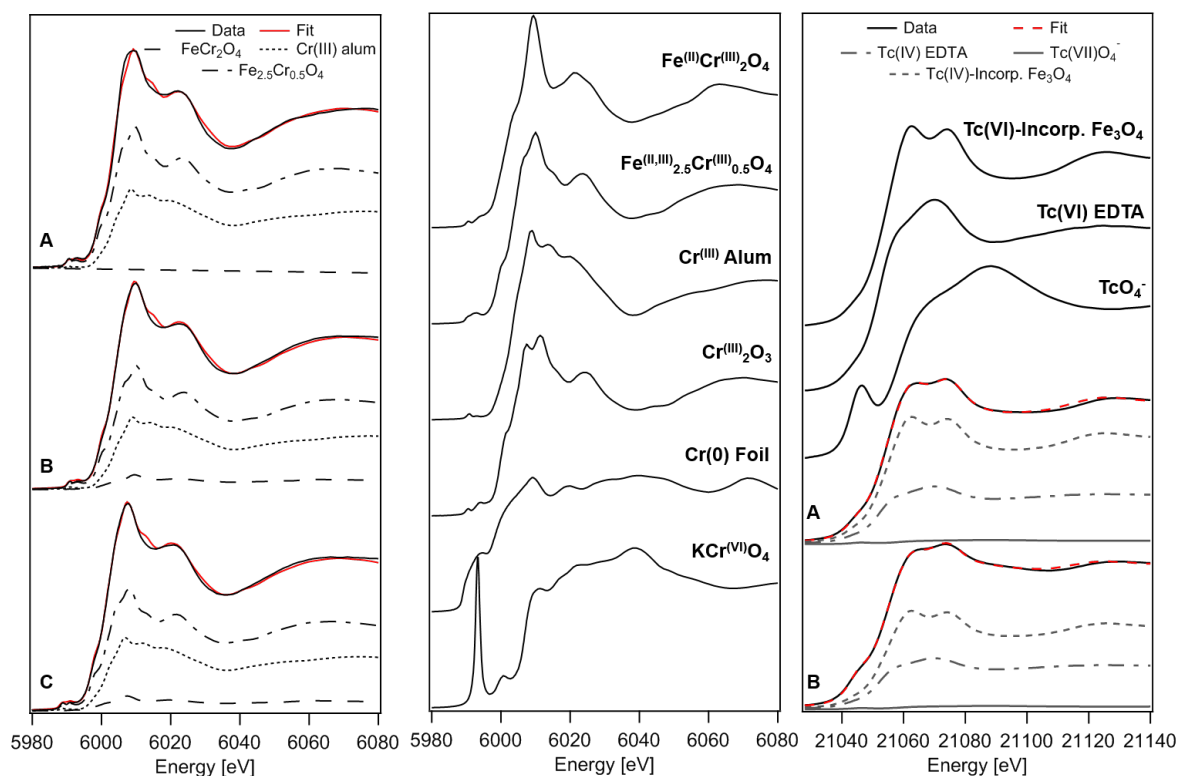


Figure 2. (Left) Normalized and off-set Cr K edge XANES spectra with corresponding LCA fits for Fe(OH)₂(s):Simulant ratios (A) 200 g/L, 100 ppm Tc(VII), (B) 50 g/L, 100 ppm Tc(VII), and (C) 50 g/L, no Tc(VII). The LCA fit (red) to the data (black) is the sum of the standard contributions from FeCr₂O₄ (dash line), Fe_{2.5}Cr_{0.5}O₄ (dot/dash line), and Cr alum (dotted line) determined in the final fit. (Middle) Cr standards considered during LCA fitting, off-set for clarity. (Right) Normalized and off-set Tc K-edge XANES spectra (black) for samples A and B from left panel and the final Tc standards used during LCA fitting. The Tc LCA fit (red dashed line) is the sum of the standard contributions from TcO₄⁻ (line), TcEDTA (dot/dash), and Tc-incorporated Fe₃O₄ (dash).

Table 3. LCA and EXAFS Results from Cr and Tc K Edge XANES and EXAFS Spectra

Sample		LAW-50-0Tc	LAW-50-100Tc	LAW-200-100Tc
Fe(OH) ₂ (s):Simulant Ratio	g/L	50	50	200
Starting [Tc(VII)]	ppm	0	100	100
Cr XANES LCA Analysis				
Cr Alum (KCr(SO ₄) ₂ •12H ₂ O)	%	35(1)	35(1)	38(4)
	p	<0.001	<0.001	<0.001
Fe _{2.5} Cr _{0.5} O ₄	%	58(2)	59(2)	62(4)
	p	<0.001	<0.001	<0.001
FeCr ₂ O ₄	%	6(1)	6(1)	-
	p	0.287	0.304	-
Tc XANES LCA Analysis				
TcO ₄ ⁻	%	-	27.2(2)	9.0(3)
	p	-	<0.001	<0.001

Tc(IV) Incorporated Fe ₃ O ₄	%	-	49(1)	63(1)
	p	-	<0.001	<0.001
Tc(IV) EDTA	%	-	26(1)	30(1)
	p	-	<0.001	<0.001
Tc EXAFS Analysis				
TcO ₄ ⁻	%	-	33(6)	0(0)
TcO ₂ ·2H ₂ O	%	-	32(8)	67(6)
Goethite	%	-	35(3)	33(6)

Values in parenthesis indicate the standard deviation of the last significant figure.

(-) No Detected

(*) Probability that the improvement to the fit by adding the scattering shell is due to random error. A p value < 0.05 indicates that the improvement is greater than 2σ of the fit.

Cr Speciation of the Solid Surface Determined by XPS: Cr speciation was also analyzed by XPS for select solid samples. XPS analysis is specific to the top 5 – 10 nm of the sample surface; however, surface specificity may be limited here due to the small goethite crystal size (~10 nm) determined by Reitveld refinements (Table 2 **Error! Reference source not found.**). Narrow, high resolution scans for Cr are shown in Figure S2 for three Cr-containing solid samples with Fe(OH)₂(s):simulant ratios of 50, 100, and 200 g/L, where the 200 g/L sample was prepared with 100 ppm of Tc(VII). Peak fitting was performed only for the Cr 2p_{3/2} peak. A single fitting peak was used to account for surface Cr(VI), with three species considered for Cr(III): Cr₂O₃, CrOOH, and Cr(OH)₃. Chromite, FeCr₂O₄, was initially considered, but did not significantly contribute to any of the sample fits as expected based on XRD and XANES results. CrOOH accounts for Cr(III) oxyhydroxides and/or partial incorporation into goethite. A summary of the Cr-phase distribution is provided in Table 2.

From XPS survey scans it is apparent that Cr only accounts for 0.13-1.6 atomic % of the analyzed area, with Cr increasing with decreasing Fe(OH)₂(s):simulant ratio. A minor amount of Cr(VI), presumably loosely adsorbed to the sample, was detected in all samples (1.3 – 8.3 atomic %). Cr(OH)₃ was the least abundant Cr(III) species detected, decreasing from 24.7(2) atomic % to 1(2) atomic % with increasing Fe(OH)₂(s):simulant ratio. However, distribution between the

two most abundant Cr(III) species, CrOOH and Cr₂O₃, did not indicate preferential formation of one species over the other as a function of Fe(OH)₂(s):simulant ratio. Although, within error, CrOOH arguably dominates, accounting for ≤59 atomic % of surface Cr (LAW-200-100Tc). This corroborates conclusions derived from XANES analysis and suggests that Cr substitution into goethite is the favored mechanism for immobilization.

Tc Speciation Determined by XANES and XPS: The oxidation state of Tc immobilized in the solid was determined by LCA of collected Tc K-edge XANES spectra. The Tc K-edge spectra for LAW-200-100Tc and LAW-50-100Tc (Fe(OH)₂(s):simulant ratios 200 g/L and 50 g/L, respectively, each with 100 ppm of Tc(VII)) and the standards used for LCA are provided in Figure 2 (right panel). Initially, LCA considered five Tc standards: TcO₄⁻, TcEDTA,²⁴ TcO₂·xH₂O,²⁴ Tc-incorporated Fe₃O₄ (magnetite),¹² and Tc(V)POM.⁴⁶ Standards determined not to contribute significantly to the fit (value < 2σ) were removed, such that the only standards included in the final LCA fits were Tc(VII)O₄⁻, Tc(IV)-incorporated magnetite, which represents Tc(IV) in an ordered iron oxide octahedral environment (as in goethite), and Tc(IV)EDTA, which represents Tc(IV) in a disordered octahedral environment, e.g., surface sorbed, even though EDTA is not present in the sample.

With an increase in Fe(OH)₂(s), the amount of Tc(IV) incorporated into iron oxide increases from 49(1)% (LAW-50-100Tc) to 63(1)% (LAW-200-100Tc). The remaining Tc(IV), modeled as Tc(IV)EDTA, is presumably sorbed or loosely incorporated at the surface of the solid where a disordered octahedral environment would be expected. Tc(IV) EDTA contributions also remain relatively consistent between samples, 26(1)-30(1)%. Any remaining Tc is present as Tc(VII)O₄⁻ and decreases from 27.2(2)% to 9.0(3)% with increasing Fe(OH)₂(s):simulant ratio. The presence of Tc(VII) in LAW-200-100Tc is unsurprising considering a 200 g/L

Fe(OH)₂(s):simulant ratio is the requirement to remove 1 ppm of Tc(VII) from the simulant (Figure 1), not 100 ppm of Tc(VII) as present in this sample.

When Tc speciation was analyzed for LAW-200-100Tc by XPS, the results were significantly different from the bulk, with an almost equal distribution of Tc(VII) and Tc(IV) (Table 2). This difference is likely due to facile reoxidation of surface adsorbed Tc(IV) relative to Tc(IV) incorporated into the mineral. Such sensitivity to reoxidation is one difference between Tc and Cr behavior in this system, since reduction of Cr(VI) produces stable, insoluble phases including Cr(OH)₃ and Cr₂O₃ that do not require Cr incorporation into iron oxide/hydroxide phases. Additionally, these results suggest that some surface specificity is provided by XPS, despite the small goethite crystal size, or that goethite crystallites have agglomerated into larger particles. It is important to note that Tc comprises only 0.14(3) atomic % of the LAW-200-100Tc surface and was calculated while only considering Tc, Cr, Fe, O, and Cr constituents; therefore, this contribution may be in fact lower.

Local Coordination Environment of Tc in the Solid: To evaluate how Tc(IV) is immobilized in the solid, the local coordination environment of Tc in samples LAW-50-100Tc and LAW-200-100Tc was determined using EXAFS. Goethite^{39,47} and magnetite²⁵ models, modified to account for Tc substitution for Fe(III), were initially used to fit the EXAFS spectra. Difficulties distinguishing between iron oxide/hydroxide environments is not uncommon, especially when Tc(IV) is divided among several species.^{6, 27, 48-49} In addition, the local environment of Fe(III) in goethite is similar to that of the octahedral site of magnetite. In goethite, there are 4 Fe neighbors at 3.1 Å and an additional 4 Fe neighbors at 3.6 Å while in magnetite, there are 6 Fe neighbors at 3.0 Å and 6 at 3.5 Å. EXAFS analysis can determine distances more precisely (0.02 Å error) than coordination numbers (20% error). For each sample, the R-factor determined using the

magnetite model was comparable if not better than the R-factor determined using the goethite model. Furthermore, F-test results for evaluating the probability that an included scattering shell contributes significantly to the EXAFS fit (SI Table S5) also favored the magnetite model. However, given the increase in Tc-Fe bond lengths determined during fitting, which more closely match the Fe-Fe bond lengths in goethite rather than magnetite, and the results from XRD and XPS analyses, it is unlikely that magnetite is present in the solid phase. Therefore, Tc-substituted goethite is assumed to be the most representative model and accounts for 30(8)% and 33(6)% of Tc in samples LAW-50-100Tc and LAW-200-100Tc, respectively (Table 3). This distribution is lower than the range determined by XANES LCA, 49-63%, where a Tc-incorporated magnetite standard is used to account for the ordered structural environment of the iron (oxy)hydroxide phase rather than a goethite standard or model as used in the EXAFS interpretation.

In addition to goethite, including $\text{TcO}_2 \cdot 2\text{H}_2\text{O}$ into the sample fits was required to account for the portion of Tc(IV) sorbed or partially incorporated at the goethite surface. Tc(IV) sorbed as $\text{TcO}_2 \cdot 2\text{H}_2\text{O}$ requires incorporation of a Tc–Tc neighbor (bond length ~ 2.57 Å) and a long Tc–O bond (~ 2.47 Å) that accounts for the hydrated oxygen.²⁴ Although, in instances where Tc may be partially incorporated into goethite, accounting for the long Tc – O bond often does not significantly contribute to the EXAFS fit.¹⁸ With this modification to the EXAFS fit, 67(6) % of Tc was found to be present as sorbed or partially incorporated Tc(IV) in LAW-200-100Tc with the hydrated Tc-O scatter pathway contributing significantly to the fit as indicated by a p value (0.019) less than 0.05. For LAW-50-100Tc, including the long Tc–O bond did not significantly contribute to the fit, thus suggesting partial incorporation of Tc(IV) into the solid phase of up to 42(7) %. This expansion to the sample EXAFS models aligns with interpretation of the XANES

spectra, which indicated that $\geq 26\%$ of Tc(IV) is not completely incorporated into the iron oxide/hydroxide solid.

Finally, for LAW-50-100Tc, where the $\text{Fe}(\text{OH})_2(\text{s})$:simulant ratio is too low to reduce and immobilize all of the Tc present in solution, TcO_4^- was also included in the EXAFS fit and accounted for 28(3)% of bulk Tc in the solid. TcO_4^- may persist as a dissolved species in moisture retained by the sample between packaging and analysis or, if dried, as a pertechnetate salt, e.g. NaTcO_4 . Despite XANES indication LAW-200-100Tc contains 9% Tc(VII), incorporating Tc(VII) into the EXAFS fit did not significantly improve the fit. The collected EXAFS spectra, their Fourier transforms, and final fits are shown in Figure 3.

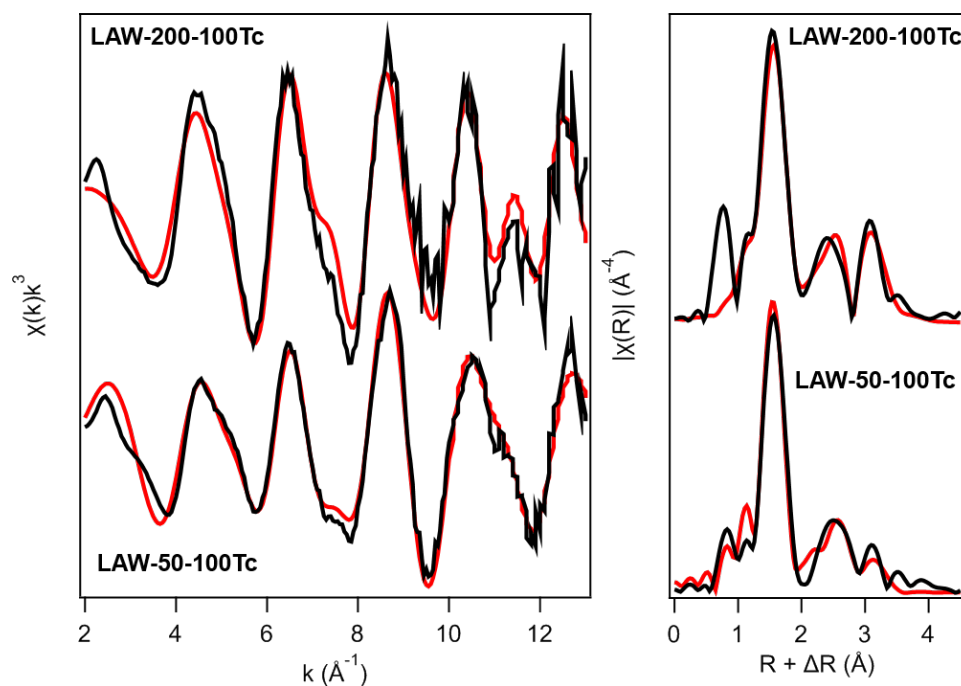


Figure 3. EXAFS spectra (left) and their Fourier transforms (right) for Tc-containing samples LAW-200-100Tc (200 g/L $\text{Fe}(\text{OH})_2(\text{s})$:simulant ratio, 100 ppm Tc(VII)) and LAW-50-100Tc (50 g/L $\text{Fe}(\text{OH})_2(\text{s})$:simulant ratio, 100 ppm Tc(VII)). EXAFS fits (red) are based on a combination of Tc-incorporated goethite, $\text{TcO}_2 \cdot 2\text{H}_2\text{O}$, and TcO_4^- (LAW-50-100Tc only) models.

4. Environmental Implications

One implication asserted after the first demonstration of Tc reduction and removal in the presence of Cr by $\text{Fe}(\text{OH})_2(\text{s})$, was that $\text{Fe}(\text{OH})_2(\text{s})$ could be introduced into Hanford LAW to form Tc-incorporated magnetite, which would stabilize Tc, decrease its volatility during vitrification, and increase Tc loading in glass waste forms.¹⁸ However, laboratory simulations of $\text{Fe}(\text{OH})_2(\text{s})$ addition to LAW indicate that the amount of $\text{Fe}(\text{OH})_2(\text{s})$ required to remove Tc and Cr is approximately one order of magnitude larger than the control system. Such a large increase in $\text{Fe}(\text{OH})_2(\text{s})$ required to address Cr and Tc in LAW may adversely affect the final glass waste form. Furthermore, under vitrification temperatures the stability of Tc is more favorable when incorporated into the iron (oxy)hydroxide phase compared to $\text{TcO}_2 \cdot 2\text{H}_2\text{O}$.⁶ As such, this system would benefit from near complete incorporation of Tc into the goethite phase, which may require additional $\text{Fe}(\text{OH})_2(\text{s})$ (>200 g/L). To this end $\text{Fe}(\text{OH})_2(\text{s})$ may be more appropriately used as a localized remediation strategy for environmental contamination or for treating the less redox-sensitive melter off-gas and secondary waste streams where the concentrations of $\text{Cr}(\text{VI})$, NO_2^- , and other anions do not overwhelm the concentration of $\text{Tc}(\text{VII})$ by orders of magnitude.

5. Supporting Information

Additional analysis procedures and results for IC/ICP-MS, XPS, and EXAFS are provided in the supporting information via the Internet at <http://pubs.acs.org>.

6. Acknowledgements

This research was supported by the U.S. Department of Energy's (DOE) Waste Treatment and Immobilization Plant Project of the Office of River Protection. PNNL is operated for the DOE by Battelle Memorial Institute under Contract DE-AC05-76RL0 1830. The XANES and EXAFS data collection was carried out at the SSRL. Use of the Stanford Synchrotron Radiation Lightsource, SLAC National Accelerator Laboratory, is supported by the U.S. Department of

Energy, Office of Science, Office of Basic Energy Sciences under Contract No. DE-AC02-76SF00515. A portion of the solid characterization was performed using EMSL and RadEMSL, a national scientific user facility sponsored by the Department of Energy's Office of Biological and Environmental Research and located at Pacific Northwest National Laboratory. A portion of this work (WWL) was supported by the U.S. Department of Energy, Office of Science, Basic Energy Sciences, Chemical Sciences, Biosciences, and Geosciences Division (CSGB), Heavy Element Chemistry Program and was performed at Lawrence Berkeley National Laboratory under contract No. DE-AC02-05CH11231. A portion of this research was also supported by the National Research Foundation of Korea (NRF) grant funded by the Korean government (No. NRF-2017K2A9A1A01093040).

7. References

1. Darab, J. G.; Smith, P. A., Chemistry of technetium and rhenium species during low-level radioactive waste vitrification. *Chemistry of Materials* **1996**, *8* (5), 1004-1021.
2. Luksic, S. A.; Riley, B. J.; Schweiger, M.; Hrma, P., Incorporating technetium in minerals and other solids: A review. *Journal of Nuclear Materials* **2015**, *466*, 526-538.
3. Banerjee, D.; Kim, D.; Schweiger, M. J.; Kruger, A. A.; Thallapally, P. K., Removal of TcO₄(-) ions from solution: materials and future outlook. *Chemical Society reviews* **2016**, *45* (10), 2724-39.
4. Zachara, J. M.; Ainsworth, C. C.; Brown, G. E.; Catalano, J. G.; McKinley, J. P.; Qafoku, O.; Smith, S. C.; Szecsody, J. E.; Traina, S. J.; Warner, J. A., Chromium speciation and mobility in a high level nuclear waste vadose zone plume. *Geochimica et Cosmochimica Acta* **2004**, *68* (1), 13-30.
5. Qafoku, O.; Pearce, C. I.; Neumann, A.; Kovarik, L.; Zhu, M.; Ilton, E. S.; Bowden, M. E.; Resch, C. T.; Arey, B. W.; Arenholz, E.; Felmy, A. R.; Rosso, K. M., Tc(VII) and Cr(VI) Interaction with Naturally Reduced Ferruginous Smectite from a Redox Transition Zone. *Environmental Science & Technology* **2017**, *51* (16), 9042-9052.
6. Um, W.; Luksic, S. A.; Wang, G.; Saslow, S.; Kim, D.-S.; Schweiger, M. J.; Soderquist, C. Z.; Bowden, M. E.; Lukens, W. W.; Kruger, A. A., Enhanced ⁹⁹Tc retention in glass waste form using Tc(IV)-incorporated Fe minerals. *Journal of Nuclear Materials* **2017**, *495* (Supplement C), 455-462.
7. Kim, D.; Kruger, A. A., Volatile species of technetium and rhenium during waste vitrification. *Journal of Non-Crystalline Solids* **2018**, *481* (Supplement C), 41-50.
8. Lee, M.-S.; Um, W.; Wang, G.; Kruger, A. A.; Lukens, W. W.; Rousseau, R.; Glezakou, V.-A., Impeding ⁹⁹Tc(IV) mobility in novel waste forms. *Nature Communications* **2016**, *7*.

9. Smith, F. N.; Um, W.; Taylor, C. D.; Kim, D. S.; Schweiger, M. J.; Kruger, A. A., Computational Investigation of Technetium(IV) Incorporation into Inverse Spinels: Magnetite (Fe_3O_4) and Trevorite (NiFe_2O_4). *Environ Sci Technol* **2016**, *50* (10), 5216-24.
10. Smith, F. N.; Taylor, C. D.; Um, W.; Kruger, A. A., Technetium Incorporation into Goethite ($\alpha\text{-FeOOH}$): An Atomic-Scale Investigation. *Environ Sci Technol* **2015**, *49* (22), 13699-707.
11. Skomurski, F. N.; Rosso, K. M.; Krupka, K. M.; McGrail, B. P., Technetium Incorporation into Hematite ($\alpha\text{-Fe}_2\text{O}_3$). *Environmental Science & Technology* **2010**, *44* (15), 5855-5861.
12. Lukens, W. W.; Magnani, N.; Tyliszczak, T.; Pearce, C. I.; Shuh, D. K., Incorporation of technetium into spinel ferrites. *Environmental Science & Technology* **2016**, *50* (23), 13160-13168.
13. Lukens, W. W.; Saslow, S. A., Aqueous Synthesis of Technetium-Doped Titanium Dioxide by Direct Oxidation of Titanium Powder, a Precursor for Ceramic Nuclear Waste Forms. *Chemistry of Materials* **2017**, *29* (24), 10369-10376.
14. Pepper, S. E.; Bunker, D. J.; Bryan, N. D.; Livens, F. R.; Charnock, J. M.; Patrick, R. A. D.; Collison, D., Treatment of radioactive wastes: An X-ray absorption spectroscopy study of the reaction of technetium with green rust. *Journal of Colloid and Interface Science* **2003**, *268* (2), 408-412.
15. Zhdanov, S., Encyclopedia of the electrochemistry of the elements. by AJ Bard, Marcel Dekker, New York **1975**, *4*, 362.
16. Rard, J. A.; Rand, M.; Anderegg, G.; Wanner, H., *Chemical thermodynamics of technetium*. Elsevier Publishing Company: 1999.
17. Russell, R. L.; Westsik Jr, J.; Swanberg, D. J.; Eibling, R. E.; Cozzi, A.; Lindberg, M. J.; Josephson, G. B.; Rinehart, D. E. *Letter report: LAW simulant development for cast stone screening tests*; Pacific Northwest National Laboratory: Richland, WA, 2013.
18. Saslow, S. A.; Um, W.; Pearce, C. I.; Engelhard, M. H.; Bowden, M. E.; Lukens, W.; Leavy, II; Riley, B. J.; Kim, D. S.; Schweiger, M. J.; Kruger, A. A., Reduction and Simultaneous Removal of ^{99}Tc and Cr by $\text{Fe}(\text{OH})_2(\text{s})$ Mineral Transformation. *Environ Sci Technol* **2017**, *51* (15), 8635-8642.
19. Gephart, R. E.; Lundgren, R. E. *Hanford tank clean up: A guide to understanding the technical issues*; PNL-10773; Pacific Northwest National Laboratory: Richland, WA., 1995; p 80.
20. Certa, P.; Empey, P.; Wells, M., River Protection Project System Plan ORP-11242 Revision 6. *Washington River Protection Solutions, LLC, Richland, Washington* **2011**.
21. Oostrom, M.; Truex, M. J.; Last, G. V.; Strickland, C. E.; Tartakovsky, G. D., Evaluation of deep vadose zone contaminant flux into groundwater: Approach and case study. *Journal of Contaminant Hydrology* **2016**, *189*, 27-43.
22. Webb, S. M., SIXpack: a graphical user interface for XAS analysis using IFEFFIT. *Physica Scripta* **2005**, *2005* (T115), 1011.
23. Ravel, B.; Newville, M., ATHENA, ARTEMIS, HEPHAESTUS: Data analysis for X-ray absorption spectroscopy using IFEFFIT. *Journal of Synchrotron Radiation* **2005**, *12* (4), 537-541.
24. Lukens, W. W.; Bucher, J. J.; Edelstein, N. M.; Shuh, D. K., Products of pertechnetate radiolysis in highly alkaline solution: Structure of $\text{TcO}_2 \cdot x\text{H}_2\text{O}$. *Environmental Science & Technology* **2002**, *36* (5), 1124-1129.

- 485 25. Wechsler, B. A.; Lindsley, D. H.; Prewitt, C. T., Crystal structure and cation distribution
486 in titanomagnetites ($\text{Fe}_{3-x}\text{Ti}_x\text{O}_4$). *American Mineralogist* **1984**, 69 (7-8), 754-770.
- 487 26. Marshall, T. A.; Morris, K.; Law, G. T. W.; Mosselmans, J. F. W.; Bots, P.; Parry, S. A.;
488 Shaw, S., Incorporation and retention of 99-Tc(IV) in magnetite under high pH conditions.
489 *Environmental Science & Technology* **2014**, 48 (20), 11853-11862.
- 490 27. Um, W.; Chang, H.-S.; Icenhower, J. P.; Lukens, W. W.; Serne, R. J.; Qafoku, N. P.;
491 Westsik, J. H.; Buck, E. C.; Smith, S. C., Immobilization of 99-technetium (VII) by Fe(II)-
492 goethite and limited reoxidation. *Environmental Science & Technology* **2011**, 45 (11), 4904-
493 4913.
- 494 28. Kendelewicz, T.; Liu, P.; Doyle, C. S.; Brown Jr, G. E., Spectroscopic study of the
495 reaction of aqueous Cr(VI) with Fe_3O_4 (111) surfaces. *Surface Science* **2000**, 469 (2-3), 144-
496 163.
- 497 29. Kendelewicz, T.; Liu, P.; Doyle, C. S.; Brown Jr, G. E.; Nelson, E. J.; Chambers, S. A.,
498 X-ray absorption and photoemission study of the adsorption of aqueous Cr(VI) on single crystal
499 hematite and magnetite surfaces. *Surface Science* **1999**, 424 (2-3), 219-231.
- 500 30. Fanning, J. C., The chemical reduction of nitrate in aqueous solution. *Coordination*
501 *Chemistry Reviews* **2000**, 199 (1), 159-179.
- 502 31. Brylev, O.; Sarrazin, M.; Roué, L.; Bélanger, D., Nitrate and nitrite electrocatalytic
503 reduction on Rh-modified pyrolytic graphite electrodes. *Electrochimica Acta* **2007**, 52 (21),
504 6237-6247.
- 505 32. Zachara, J. M.; Heald, S. M.; Jeon, B.-H.; Kukkadapu, R. K.; Liu, C.; McKinley, J. P.;
506 Dohnalkova, A. C.; Moore, D. A., Reduction of pertechnetate [Tc(VII)] by aqueous Fe(II) and
507 the nature of solid phase redox products. *Geochimica et Cosmochimica Acta* **2007**, 71 (9), 2137-
508 2157.
- 509 33. Wells, M.; Fitzpatrick, R. W.; Gilkes, R., Thermal and mineral properties of Al-, Cr-,
510 Mn-, Ni- and Ti-substituted goethite. *Clays and Clay Minerals* **2006**, 54 (2), 176-194.
- 511 34. Schikorr, G., Über die Reaktionen zwischen Eisen, seinen Hydroxyden und Wasser.
512 *Zeitschrift für Elektrochemie und angewandte physikalische Chemie* **1929**, 35 (2), 65-70.
- 513 35. He, Y. T.; Traina, S. J., Cr(VI) Reduction and Immobilization by Magnetite under
514 Alkaline pH Conditions: The Role of Passivation. *Environmental Science & Technology* **2005**,
515 39 (12), 4499-4504.
- 516 36. Jolivet, J.-P.; Chanéac, C.; Tronc, E., Iron oxide chemistry. From molecular clusters to
517 extended solid networks. *Chemical Communications* **2004**, (5), 481-483.
- 518 37. Um, W.; Chang, H.; Icenhower, J. P.; Lukens, W. W.; Jeffrey Serne, R.; Qafoku, N.;
519 Kukkadapu, R. K.; Westsik, J. H., Iron oxide waste form for stabilizing 99Tc. *Journal of Nuclear*
520 *Materials* **2012**, 429 (1-3), 201-209.
- 521 38. Shannon, R., Revised effective ionic radii and systematic studies of interatomic distances
522 in halides and chalcogenides. *Acta Crystallographica Section A* **1976**, 32 (5), 751-767.
- 523 39. Schwertmann, U.; Gasser, U.; Sticher, H., Chromium-for-iron substitution in synthetic
524 goethites. *Geochimica et Cosmochimica Acta* **1989**, 53 (6), 1293-1297.
- 525 40. Shannon, R. D.; Prewitt, C. T., Effective ionic radii in oxides and fluorides. *Acta*
526 *Crystallographica Section B* **1969**, 25 (5), 925-946.
- 527 41. Fazey, P.; O'Connor, B.; Hammond, L., X-ray powder diffraction Rietveld
528 characterization of synthetic aluminum-substituted goethite. *Clays and Clay Minerals* **1991**, 39
529 (3), 248-253.

42. Alvarez, M.; Rueda, E. H.; Sileo, E. E., Simultaneous incorporation of Mn and Al in the goethite structure. *Geochimica et Cosmochimica Acta* **2007**, *71* (4), 1009-1020.
43. Farges, F., Chromium speciation in oxide-type compounds: application to minerals, gems, aqueous solutions and silicate glasses. *Phys Chem Minerals* **2009**, *36* (8), 463-481.
44. Nyburg, S. C.; Steed, J. W.; Aleksovska, S.; Petrusevski, V. M., Structure of the alums. I. On the sulfate group disorder in the [alpha]-alums. *Acta Crystallographica Section B* **2000**, *56* (2), 204-209.
45. Giovanoli, R.; Stadelmann, W.; Feitknecht, W., Über kristallines Chrom (III) hydroxid. I. *Helvetica Chimica Acta* **1973**, *56* (3), 839-847.
46. McGregor, D.; Burton-Pye, B. P.; Howell, R. C.; Mbomekalle, I. M.; Lukens, W. W.; Bian, F.; Mausolf, E.; Poineau, F.; Czerwinski, K. R.; Francesconi, L. C., Synthesis, Structure Elucidation, and Redox Properties of ⁹⁹Tc Complexes of Lacunary Wells–Dawson Polyoxometalates: Insights into Molecular ⁹⁹Tc–Metal Oxide Interactions. *Inorganic Chemistry* **2011**, *50* (5), 1670-1681.
47. Szytuła, A.; Burewicz, A.; Dimitrijević, Ž.; Kraśnicki, S.; Rżany, H.; Todorović, J.; Wanic, A.; Wolski, W., Neutron Diffraction Studies of α-FeOOH. *physica status solidi (b)* **1968**, *26* (2), 429-434.
48. Peretyazhko, T.; Zachara, J. M.; Heald, S. M.; Jeon, B. H.; Kukkadapu, R. K.; Liu, C.; Moore, D.; Resch, C. T., Heterogeneous reduction of Tc(VII) by Fe(II) at the solid–water interface. *Geochimica et Cosmochimica Acta* **2008**, *72* (6), 1521-1539.
49. Masters-Waage, N. K.; Morris, K.; Lloyd, J. R.; Shaw, S.; Mosselmans, J. F. W.; Boothman, C.; Bots, P.; Rizoulis, A.; Livens, F. R.; Law, G. T. W., Impacts of Repeated Redox Cycling on Technetium Mobility in the Environment. *Environmental Science & Technology* **2017**, *51* (24), 14301-14310.

556 Tables.

557 **Table 1.** 5 M Na Average LAW Simulant Composition

Constituent	Target Concentration [mg/L] [*]	Concentration [mg/L]	Constituent	Target Concentration [mg/L] [*]	Concentration [mg/L]
Al	8280	8500	F ⁻	600	<1000
Cr	1120	1080	Cl ⁻	1500	<2500
P	1520	981	NO ₂ ⁻	26,000	26,800
K	1280	1300	Br ⁻	-	<5000
Na	115,000	110,000	NO ₃ ⁻	101,000	102,000
S	2740	2810	SO ₄ ⁻	-	10,100
Ti	-	7.84	PO ₄ ⁻	-	<7500
pH		13.5			

^{*} Target Concentrations from Russell et al, 2013.¹⁷

-: Not identified

558

559 **Table 2.** XRD and High Resolution XPS Analysis of Select Solid Phases

Sample		LAW-50-0Tc-1	LAW-100-0Tc	LAW-200-100Tc
Fe(OH) ₂ (s):Simulant Ratio	g/L	50	100	200
Starting [Tc(VII)]	ppm	0	0	100
XRD Analysis				
Goethite (α -FeOOH)	wt%	77	81	-
a	(\AA) [*]	4.602(2)	4.597(3)	-
b	(\AA) [*]	9.920(3)	9.913(2)	-
c	(\AA) [*]	3.0096(9)	3.0080(9)	-
Crystal Size	(nm) ^{**}	9.8(1)	10.7(1)	-
Feroxyhyte (δ -FeOOH)	wt%	17	14	-
Hematite (Fe ₂ O ₃)	wt%	-	3	-
Amorphous/Unidentified	wt%	6	1	-
Survey XPS Analysis ^{**}				
Cr 2p	at % [*]	1.6(1)	1.1(1)	0.13(1)
Tc 3d	at %	-	-	0.14(3)
Fe 2p	at %	7.3(4)	8.4(8)	1.7(2)
C 1s	at %	27(4)	19(6)	24(1)
O 1s	at %	64(3)	71(5)	74(1)
Cr XPS Analysis ^{**}				
CrOOH	at %	46(1)	38(14)	59(2)
Cr ₂ O ₃	at %	28(10)	43(19)	32(4)
Cr(OH) ₃	at %	24.7(2)	18(5)	1(2)
Cr(VI)	at %	1.5	1.3(5)	8.3(8)
Tc XPS Analysis ^{**}				
Tc(VII)	at %	-	-	52(1)
Tc(IV)	at %	-	-	48(1)
Fe XPS Analysis ^{**}				
FeCr ₂ O ₄	at %	0	0	5.7(2)
Fe ₃ O ₄	at %	12(1)	11(2)	11(1)
FeOOH	at %	88(1)	89(2)	83(1)

(-) No Detected or Analyzed (*) Atomic percent

Goethite (α -FeOOH)³³: a = 4.634 Å, b = 9.945 Å, c = 3.0321 Å

*Values in parentheses are $\pm 3\sigma$, based on the error associated with the Reitveld refinement.

**Values in parentheses are $\pm 1\sigma$. For XPS, the standard deviation is determined from the average of two replicate spot analyses collected for each sample.

Table 3. LCA and EXAFS Results from Cr and Tc K Edge XANES and EXAFS Spectra

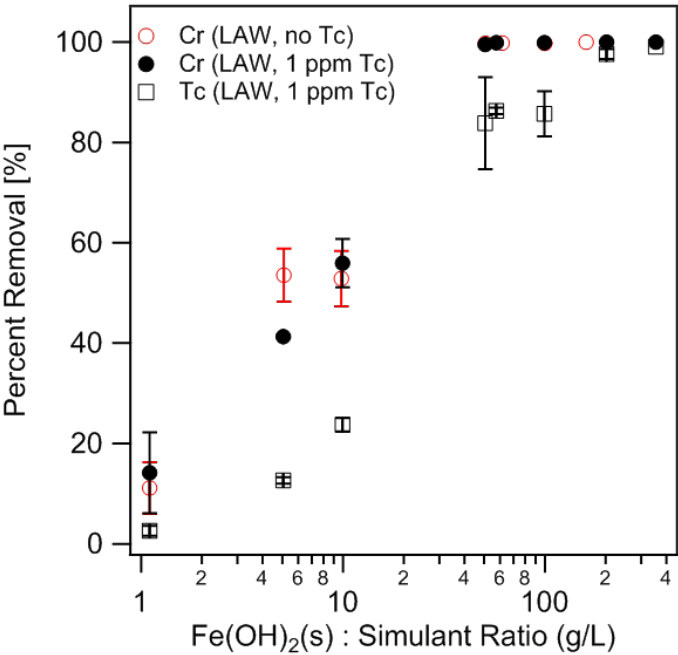
Sample		LAW-50-0Tc	LAW-50-100Tc	LAW-200-100Tc
Fe(OH) ₂ (s):Simulant Ratio	g/L	50	50	200
Starting [Tc(VII)]	ppm	0	100	100
Cr XANES LCA Analysis				
Cr Alum (KCr(SO ₄) ₂ •12H ₂ O)	%	35(1)	35(1)	38(4)
	p*	<0.001	<0.001	<0.001
Fe _{2.5} Cr _{0.5} O ₄	%	58(2)	59(2)	62(4)
	p	<0.001	<0.001	<0.001
FeCr ₂ O ₄	%	6(1)	6(1)	-
	p	0.287	0.304	-
Tc XANES LCA Analysis				
TcO ₄ ⁻	%	-	27.2(2)	9.0(3)
	p	-	<0.001	<0.001
Tc(IV) Incorporated Fe ₃ O ₄	%	-	49(1)	63(1)
	p	-	<0.001	<0.001
Tc(IV) EDTA	%	-	26(1)	30(1)
	p	-	<0.001	<0.001
Tc EXAFS Analysis				
TcO ₄ ⁻	%	-	33(6)	0(0)
TcO ₂ •2H ₂ O	%	-	32(8)	67(6)
Goethite	%	-	35(3)	33(6)

Values in parenthesis indicate the standard deviation of the last significant figure.

(-) No Detected

(*) Probability that the improvement to the fit by adding the scattering shell is due to random error. A p value < 0.05 indicates that the improvement is greater than 2σ of the fit.

564 Figures.
565



566
567 **Figure 1.** Cr and Tc removal from LAW simulant with 1 ppm Tc (black) and without Tc (red).
568 Cr(VI) results are indicated by filled circles, Tc results by open squares. Error bars represent the
569 standard deviation of results averaged from two to six replicate samples. Percent removal
570 assumed to be 100% if below ICP-OES detection limit for Cr (23 $\mu\text{g/L}$) or ICP-MS detection
571 limit for Tc (33 ng/L).

572
573

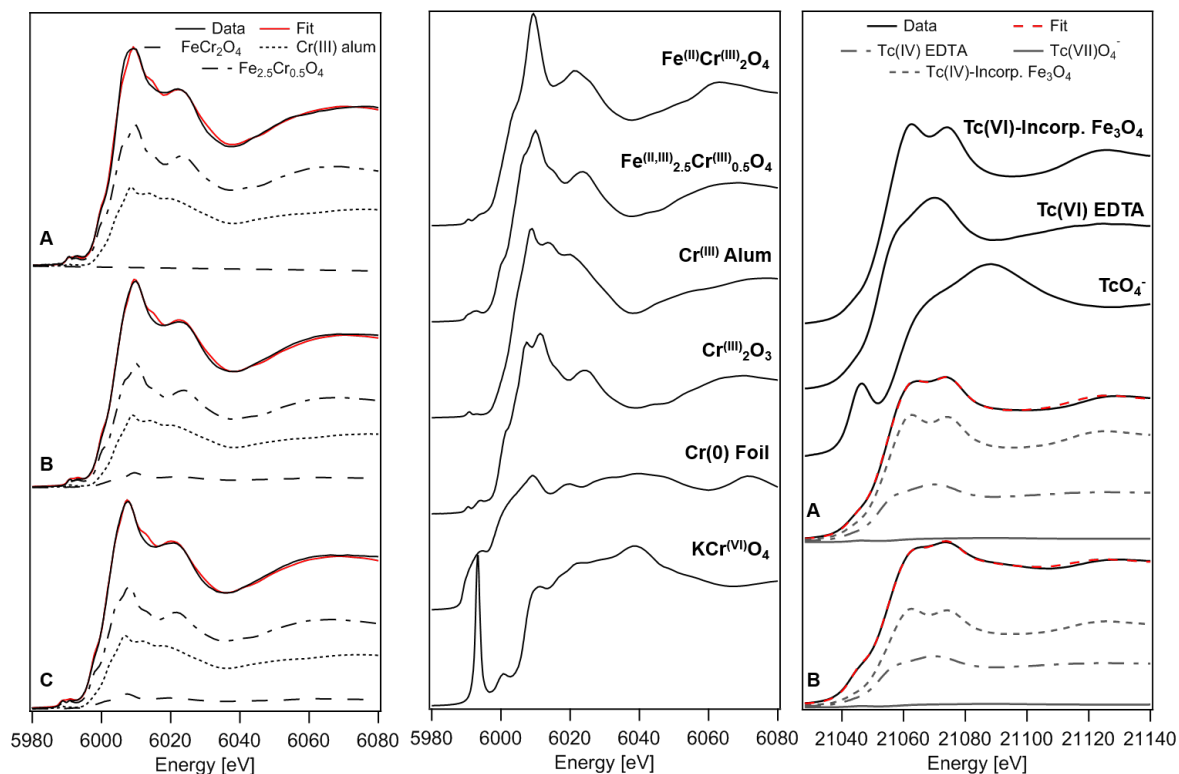


Figure 2. (Left) Normalized and off-set Cr K edge XANES spectra with corresponding LCA fits for $\text{Fe(OH)}_2(\text{s})$:Simulant ratios (A) 200 g/L, 100 ppm Tc(VII), (B) 50 g/L, 100 ppm Tc(VII), and (C) 50 g/L, no Tc(VII). The LCA fit (red) to the data (black) is the sum of the standard contributions from FeCr_2O_4 (dash line), $\text{Fe}_{2.5}\text{Cr}_{0.5}\text{O}_4$ (dot/dash line), and Cr alum (dotted line) determined in the final fit. (Middle) Cr standards considered during LCA fitting, off-set for clarity. (Right) Normalized and off-set Tc K-edge XANES spectra (black) for samples A and B from left panel and the final Tc standards used during LCA fitting. The Tc LCA fit (red dashed line) is the sum of the standard contributions from TcO_4^- (line), TcEDTA (dot/dash), and Tc-incorporated Fe_3O_4 (dash).

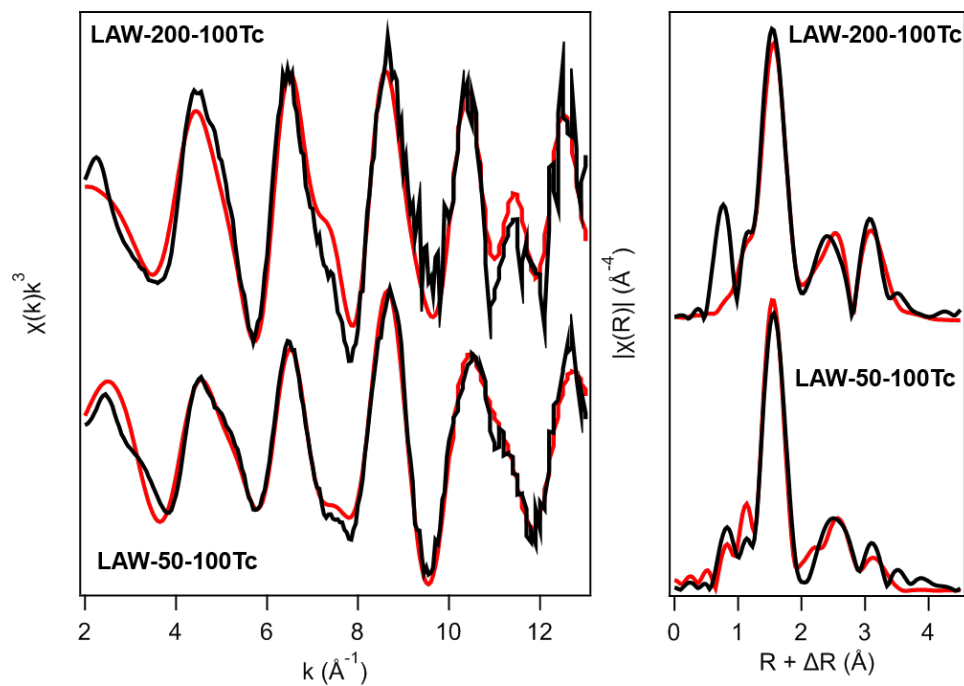


Figure 3. EXAFS spectra (left) and their Fourier transforms (right) for Tc-containing samples LAW-200-100Tc and LAW-50-100Tc. EXAFS fits (red) are based on a combination of Tc-incorporated goethite, $\text{TcO}_2 \cdot 2\text{H}_2\text{O}$, and TcO_4^- (LAW-50-100Tc only) models.